Journal of Alloys and Compounds 509S (2011) S817–S822

Contents lists available at ScienceDirect

Journal of Alloys and Compounds

journal homepage: www.elsevier.com/locate/jallcom

High pressure *in situ* diffraction studies of metal–hydrogen systems

V.A. Yartys[a,b,*], R.V. Denys[a,c], C.J. Webb[d], J.P. Mæhlen[a], E. MacA. Gray[d], T. Blach[d], O. Isnard[e], L.C. Barnsley[d]

[a] *Institute for Energy Technology, Kjeller NO 2027, Norway*
[b] *Norwegian University of Science and Technology, Trondheim NO 7491, Norway*
[c] *Karpenko Physico-Mechanical Institute, NAS of Ukraine, Lviv 79601, Ukraine*
[d] *Queensland Micro- and Nanotechnology Centre, Griffith University, Australia*
[e] *Institute Néel, CNRS/UJF, 38042 Grenoble, France*

ARTICLE INFO

Article history:
Received 19 November 2010
Received in revised form 2 December 2010
Accepted 3 December 2010
Available online 10 December 2010

Keywords:
Metal hydride
Cerium
Zirconium
High pressure hydrogen
Neutron powder diffraction
Pressure–composition–temperature diagrams

ABSTRACT

"Hybrid" hydrogen storage, where hydrogen is stored in both the solid material and as a high pressure gas in the void volume of the tank can improve overall system efficiency by up to 50% compared to either compressed hydrogen or solid materials alone. Thermodynamically, high equilibrium hydrogen pressures in metal–hydrogen systems correspond to low enthalpies of hydrogen absorption–desorption. This decreases the calorimetric effects of the hydride formation–decomposition processes which can assist in achieving high rates of heat exchange during hydrogen loading—removing the bottleneck in achieving low charging times and improving overall hydrogen storage efficiency of large hydrogen stores. Two systems with hydrogenation enthalpies close to −20 kJ/mol H_2 were studied to investigate the hydrogenation mechanism and kinetics: $CeNi_5$–D_2 and $ZrFe_{2-x}Al_x$ (x = 0.02; 0.04; 0.20)–D_2. The structure of the intermetallics and their hydrides were studied by *in situ* neutron powder diffraction at pressures up to 1000 bar and complementary X-ray diffraction. The deuteration of the hexagonal $CeNi_5$ intermetallic resulted in $CeNi_5D_{6.3}$ with a volume expansion of 30.1%. Deuterium absorption filled three different types of interstices, Ce_2Ni_2 and Ni_4 tetrahedra, and Ce_2Ni_3 half-octahedra and was accompanied by a valence change for Ce. Significant hysteresis was observed between deuterium absorption and desorption which profoundly decreased on a second absorption cycle.

For the Al-modified Laves-type C15 $ZrFe_{2-x}Al_x$ intermetallics, deuteration showed very fast kinetics of H/D exchange and resulted in a volume increase of the FCC unit cells of 23.5% for $ZrFe_{1.98}Al_{0.02}D_{2.9(1)}$. Deuterium content, hysteresis of H/D uptake and release, unit cell expansion and stability of the hydrides systematically change with the amount of Al content. In the deuteride D atoms exclusively occupy the $Zr_2(Fe,Al)_2$ tetrahedra. Observed interatomic distances are Zr–D = 1.98–2.11; (Fe, Al)–D = 1.70–1.75 Å. Hydrogenation slightly increases the magnetic moment of the Fe atoms in $ZrFe_{1.98}Al_{0.02}$ and $ZrFe_{1.96}Al_{0.04}$ from 1.9 μ_B at room temperature for the alloy to 2.2 μ_B for its deuteride.

1. Introduction

"Hybrid" H storage combines metal hydrides (MH) and compressed hydrogen gas and yields an improvement of up to 50% in the overall H storage system efficiency [1]. This paper presents the data of the high pressure studies of metal hydrogen systems where the hydrogen storage capacity of the MH is significantly pressure-dependent as H_2 pressures increase to a few hundred bar.

The kinetics of hydrogen absorption and desorption and phase-structural characterization of the systems can be efficiently performed by *in situ* diffraction studies. Using deuterated samples and neutron scattering in pressure cells filled with deuterium gas allows us to probe the H/D environment and to study the metal–H/D and H–H/D–D interactions via investigations of the pressure-dependant changes of the phase-structural composition of the materials. Obviously there are technical challenges with this kind of work. Thus, the range of particular metal hydride systems studied by *in situ* NPD at high D_2 pressures is rather limited. In earlier research, much of the focus was on the $LaNi_5$–D_2 and Pd–D_2 systems where systematic studies under high pressure experimental conditions were performed (see [2,3] as examples).

Broader studies of the different materials are required for better understanding the behaviour of the high pressure hydrides. The present work was aimed at investigating the hydrides

* Corresponding author at: Institute for Energy Technology, Instituttveien 18, P.O. Box 40, NO 2027 Kjeller, Norway. Tel.: +47 63806453; fax: +47 63812905.
E-mail address: volodymyr.yartys@ife.no (V.A. Yartys).

0925-8388/$ – see front matter © 2010 Elsevier B.V. All rights reserved.
doi:10.1016/j.jallcom.2010.12.030

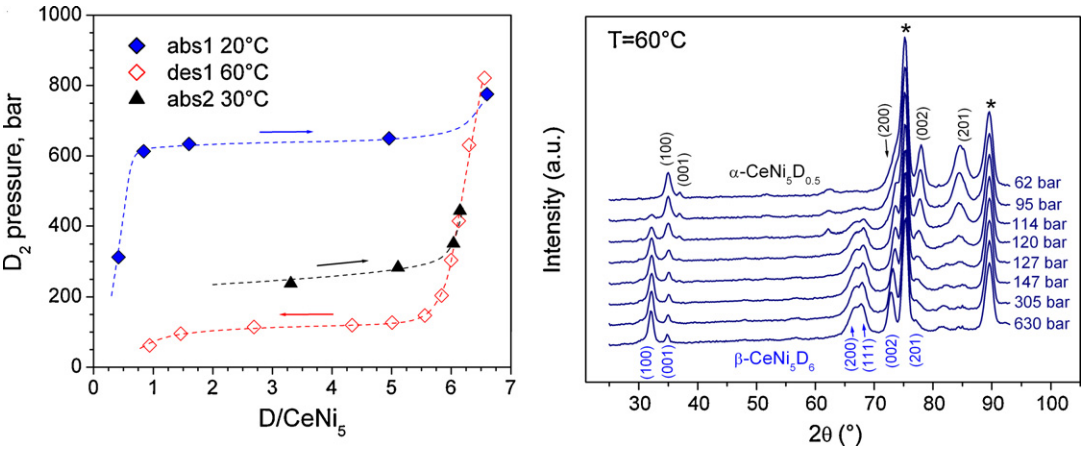

Fig. 1. (a) P–C diagrams for $CeNi_5$–D_2 system obtained by volumetric measurements during *in situ* NPD experiments; (b) evolution of NPD pattern during deuterium desorption (des1 60 °C) in $CeNi_5$–D_2 system. The asterisks show reflections from a stainless steel liner of the high-pressure sample cell.

belonging to the two most commonly used groups of the hydrogen storage intermetallics, $CaCu_5$-type and Laves-phase compounds.

A structural analogue of the La-containing intermetallic, $CeNi_5$–D_2 system was studied by *in situ* NPD at pressures up to 1000 bar. The Zr-based Laves phase compounds $ZrFe_2$ and $ZrCo_2$ can be hydrogenated only using high applied hydrogen pressures, up to 3000 bar, giving $ZrFe(Co)_2D_{\sim 3}$ [4]. These deuterides were studied *ex situ* by NPD and their crystal structures were solved. Al substitution for Fe in $ZrFe_2$ significantly modifies the hydrogenation behaviour decreasing the equilibrium pressure of hydrogen and increasing stability of the hydride [5]. The range of studied $ZrFe_{2-x}Al_x$ materials was limited to alloys with a rather large content of Al; thus, the equilibrium pressures of hydrogen desorption were well below 100 bar [5]. In the present work we focused on the experimental study of the systems in which the Al content was very low, below 0.2 at.Al/f.u. $Zr(Fe,Al)_2$, thus aiming to synthesize hydrides where the stability was expected to be only slightly increased as compared to $ZrFe_2$–H_2 system. The *in situ* NPD studies were performed at pressures up to 1000 bar.

2. Experimental details

The $CeNi_5$ and $Zr(Fe,Al)_2$ alloys were prepared from the individual constituent metals, Ce, Zr, Ni, Fe and Al with a purity of at least 99.9%, by arc melting in argon gas on a water cooled copper pad. X-ray diffraction studies (Siemens D 5000 diffractometer, Cu $K\alpha_1$ radiation) showed that the prepared samples were single phases intermetallics with $CaCu_5$-type ($CeNi_5$) and $MgCu_2$ [$Zr(Fe,Al)_2$] type of structures. Powder diffraction data were analysed by the Rietveld whole-profile refinement method with Fullprof [6].

Powder neutron diffraction data were collected with the D1B diffractometer at ILL, Grenoble ($\lambda = 2.52$ Å). The experimental setup for the *in situ* NPD study consisted of a high-pressure Sieverts manometric hydrogenator connected to a high-pressure sample cell made of a zero coherent scattering alloy (Zr–Ti) with a thin stainless steel inner liner. High pressures were achieved by the use of multistage, heat-based deuterium intensifier (maximum H_2 pressure 2 kbar). The *in situ* apparatus allowed simultaneous measurement of PCT diagrams of the metal–deuterium systems and assessment of the crystal structure via neutron diffraction. A detailed description of the hydrogenation setup is given in [7].

Measurements of magnetization were taken from an in-house built vibrating sample magnetometer. Powder samples were packed under argon into sealed Kel-F sample containers. Zero-field cooled and field cooled temperature dependent magnetizations were measured on these samples from 4 K to 315 K at 100 Oe and 1000 Oe. Magnetic hysteresis loops were measured between ±6 kOe at 315 K and 4.1 K and the values of saturation magnetization were taken from these hysteresis loops.

3. Results and discussion

3.1. $CeNi_5$–D_2 system

The initial intermetallic $CeNi_5$ alloy was characterized by SR XRD (SNBL; BM01A; $\lambda = 0.7350$ Å) as a single phase sample containing the $CeNi_5$ intermetallic compound with a hexagonal unit cell: $a = 4.88415(7)$; $c = 4.00016(7)$ Å. The first deuteration was tried without preliminary activation of the alloy and took place on application of high deuterium pressures. Our observations of the absorption–desorption processes can be summarized as follows:

- Both deuterium absorption and desorption are characterized by a presence of clear plateaux on the P–C diagrams (Fig. 1a).
- A solid solution of deuterium in $CeNi_5$, α-$CeNi_5D_{\sim 0.5}$, is formed first and extends until the level of pressure of 600 bar D_2. At higher deuterium pressures the α-$CeNi_5D_{\sim 0.5} \rightarrow \beta$-$CeNi_5D_{\sim 6}$ transformation takes place.
- During the first deuteration, the midpoint of the $\alpha \rightarrow \beta$ plateau at 20 °C is observed at 632 bar D_2; maximum D content in the saturated beta deuteride, according to the manometric measurements, equals to 6.5 at.D/f.u. at ~800 bar D_2.
- During the deuterium desorption, the midpoint of the plateau pressure for the $\beta \rightarrow \alpha$ transformation is observed at significantly lower pressure, 117 bar D_2 at 60 °C. Changes of the NPD pattern during the D_2 desorption are shown in Fig. 1b.
- During the second deuteration, a midplateau pressure for the $\alpha \rightarrow \beta$ transformation at 30 °C is significantly decreased, to just 237 bar D_2.
- The significant hysteresis in deuterium absorption/desorption observed in this work is in agreement with the reference data for the corresponding hydride [8].

3.1.1. α-$CeNi_5D_{0.5}$

During the formation of the α-solid solution, the original hexagonal unit cell slightly expands; $\Delta a/a = 0.3\%$; $\Delta c/c = 0.6\%$; $\Delta V/V = 1.1\%$; $a = 4.8969(6)$; $c = 4.0261(6)$ Å; $V = 83.61(2)$ Å^3 (data collected at D1B with $\lambda = 2.52$ Å). From Rietveld profile refinements of the NPD data we conclude that in the alpha solid solution D atoms exclusively occupy the Ce_2Ni_2 tetrahedral site (6m). The refined positional parameters for D atoms [$x = 0.118(5)$; $y = 2x$; $z = 1/2$; $n = 0.085(7)$] indicate that they are located close to the centres of the tetrahedra. Interestingly, only this Ce_2Ni_2 interstitial site meets the requirements from the geometrical criterion for the sizes

of the H-occupied sites, namely radius >0.4 Å. For Ce_2Ni_2, $r = 0.42$ Å, all the other sites have radii below 0.3 Å and thus remain vacant.

It is worth pointing out a difference in the site occupancies between the α-$LaNi_5D_{0.42}$ [9] and α-$CeNi_5D_{0.5}$ solid solutions. Indeed, in the $LaNi_5$-based solid solution D atoms occupy two different sites, 6m (~2%) and 12n (3%), in contrast to the α-$CeNi_5D_{0.5}$ where only the 6m sites are partially filled. From volumetric data of the D absorption capacity, the limiting D content in the α-solid solution is higher for the Ce-containing α-$RENi_5D_x$, 0.84 at.D/$CeNi_5$, as compared to the La-containing solution, $x = 0.42$.

Furthermore, we observe a small difference between the data of the volumetric measurements and the results of the crystal structure refinements. This difference can be caused by a presence of undistinguishable amounts of the β-deuteride (ca. 5%) in the sample already at 613 bar D_2. Such small quantities are difficult to confidently identify using the NPD data with a lower resolution, as at the D1B instrument. However, the high flux beam allowed fast collection of a single data set, on a time scale of approximately 2 min, allowing kinetic measurements of the processes of phase-structural transformations caused by absorption or desorption of deuterium gas.

3.1.2. β-$CeNi_5D_{6.3}$

NPD data showed complete transformation into the β-deuteride at D_2 pressure of 776 bar. During the deuteration, the unit cell expands by 30.1%, with $\Delta a/a = 10.0\%$ and $\Delta c/c = 7.5\%$. Volume expansion during the formation of the β-$CeNi_5D_{6.3}$ is significantly larger as compared to $LaNi_5D_{6.5}$ (~24%) [10]. No superstructure peaks were observed in the NPD pattern; thus, the structure of the $CeNi_5D_{6.3}$ deuteride was described in the space group *P*6/*mmm*. However, we cannot exclude possible hydrogen ordering in the structure resulting in a doubling of the unit cell and lowering of the symmetry, similar as in the β-$LaNi_5D_{6+x}$ [11]. The limited resolution of the obtained NPD data did not allow for this to be verified.

The refinements in the sp.gr. *P*6/*mmm* yielded a satisfactory fit between the experimental and calculated data (see Fig. 2). Three different interstitial sites were found to be partially filled by D atoms, including Ce_2Ni2_2 tetrahedra 6m; $Ce_2Ni1_2Ni_2$ sites 6i (half of the octahedron $Ce_2Ni1_2Ni_2$) and tetrahedra Ni_4 4 h. Refined deuterium content of 6.3(2) at.D/f.u. well agrees with the volumetric measurements, 6.5 D/f.u. The crystal structure of $CeNi_5D_{6.3}$ deuteride is shown in Fig. 3. The crystal structure data for the $CeNi_5D_{6.3}$ are presented in Table 1.

We note that the values of the unit cell parameters for the saturated $CeNi_5D_{6.3}$ deuteride, $a = 5.374(2)$; $c = 4.3012(7)$ Å, are very close to the corresponding values for $LaNi_5D_6$ [9]. This is in contrast to a significant difference between the sizes of the unit cells for $LaNi_5$ and $CeNi_5$, where a significant contraction of the unit cells takes place on a replacement of La by Ce. Thus, a decrease of the Ce valence from a partial 4+ state in $CeNi_5$ to a trivalent state in $CeNi_5D_{6.3}$ is likely to take place during the hydrogenation process.

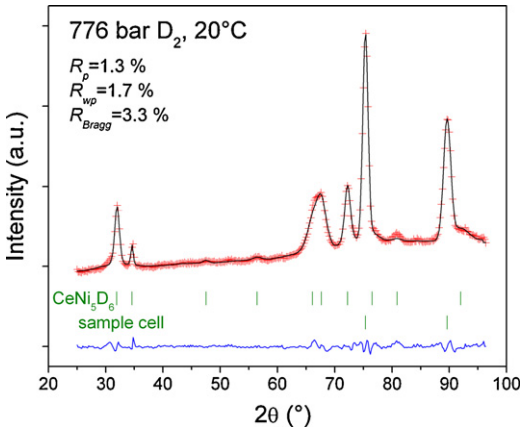

Fig. 2. Refined neutron diffraction pattern for $CeNi_5D_{6.3}$ (observed (+), calculated (—) and difference (bottom line) profiles).

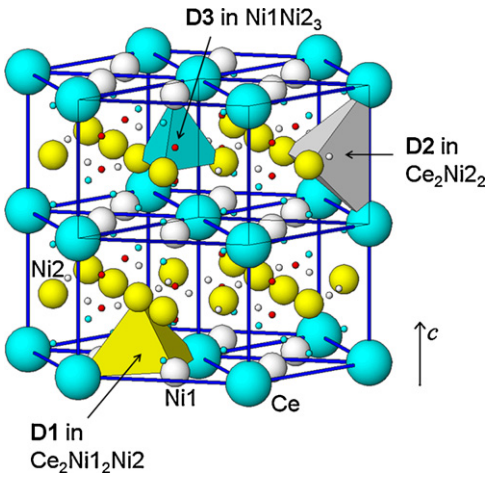

Fig. 3. Crystal structure of the $CeNi_5D_{6.3}$ deuteride. Three types of interstices occupied by D atoms are shown.

It should be noted that without use of *in situ* diffraction applied in the present work it is not possible to measure the correct crystallographic data for the saturated deuteride. Indeed, in the work [8] where a high pressure $CeNi_5$-based hydride was stabilized by SO_2, before performing the *ex situ* diffraction data, the experimentally measured values of the unit cell parameters were much smaller ($a = 5.368$; $c = 4.235$ Å) as compared to the present study ($a = 5.374(2)$; $c = 4.3012(7)$ Å) indicating a possible partial H desorption from the sample following a pressure decrease within the homogeneity range of the β-hydride.

Finally, we have observed a pronounced anisotropic diffraction peak broadening upon the first hydrogenation of the $CeNi_5$, during

Table 1
Crystallographic data for the β-$CeNi_5D_{6.3(2)}$ (20 °C, 776 bar D_2) deuteride. Sp.gr. *P*6/*mmm*; $a = 5.374(2)$; $c = 4.3012(7)$ Å; $V = 107.56(5)$ Å^3. Isotropic atomic displacement factors B_{iso} were fixed for Ce (1.0 Å^2), Ni (1.0 Å^2) and D (2.0 Å^2).

Atom	Site	*x*/*a*	*y*/*b*	*z*/*c*	Occupancy, at.D/unit cell	Interatomic Me–D distances, Å
Ce	1a	0	0	0		
Ni1	2b	1/3	2/3	0		
Ni2	3g	1/2	0	1/2		
D1	6i	1/2	0	0.143(3)	2.99(10) filled 50%	Ce–D1 2.76 Ni1–D1 1.67 Ni2–D1 1.54
D2	6m	0.136(2)	0.272(4)	1/2	2.64(8) filled 44%	Ce–D2 2.50 Ni2–D2 1.71
D3	4h	1/3	2/3	0.380(–)	0.62(4) filled 16%	Ni1–D3 1.63 Ni2–D3 1.63

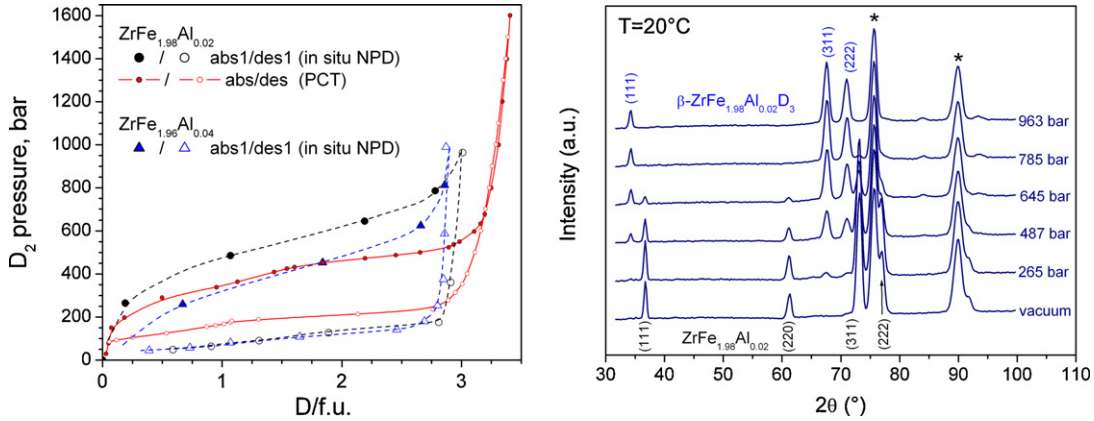

Fig. 4. (a) P–C diagrams measured at room temperature for the first D_2 absorption–desorption cycle in the $ZrFe_{2-x}Al_x$–D_2 systems. The data are collected by the volumetric measurements during *in situ* NPD experiments. Absorption–desorption isotherms for the activated $ZrFe_{1.98}Al_{0.02}$ were obtained during the conventional PCT measurements and are given for comparison. (b) Evolution of the NPD pattern during deuterium absorption by $ZrFe_{1.98}Al_{0.02}$. The asterisks show the peaks from the high-pressure sample cell.

the α-$CeNi_5D_{\sim 0.5} \rightarrow \beta$-$CeNi_5D_{\sim 6}$ transformation. The anisotropic strain broadening is not observed in the initial period of the hydrogenation, until the β-deuteride appears and, after that, remains a component of the metal–hydrogen system during further desorption–absorption cycling. Similar effect was observed during the cycling in hydrogen gas of $LaNi_5$ [2,12] and its related substituted $LaNi_{5-x}M_x$ (M = Co, Mn, Al, Fe, Cu, Sn) [14]. Such an anisotropic broadening is attributed to misfit dislocations created during the first hydrogenation [13,14]. During the refinements, the anisotropic peak broadening was modelled using the function developed by Latroche et al. [15], where it is described as originating from the local variations of the unit cell parameters *a* and *c* of the hexagonal cells, using three microstrain coefficients S_{AA}, S_{CC} and C_{AC}. The strain coefficients obtained in this work for the $CeNi_5D_{6.3}$ are $S_{AA} = 1.14 \cdot 10^{-3}$ Å^{-2} and $S_{CC} = 0.3 \cdot 10^{-3}$ Å^{-2} (correlation parameter C_{AC} was fixed to 1.0) and are comparable with those reported for the $LaNi_5D_{6.5}$ deuteride ($S_{AA} = 0.79 \cdot 10^{-3}$ Å^{-2} and $S_{CC} = 0.08 \cdot 10^{-3}$ Å^{-2}) [9] or for $LaNi_5$ after several absorption–desorption cycles ($S_{AA} = 0.76 \cdot 10^{-3}$ Å^{-2} and $S_{CC} = 0.22 \cdot 10^{-3}$ Å^{-2}) [14]. As suggested in [9,14], a decrease in the discrete unit cell volume expansion values during the $\alpha \rightarrow \beta$ transition in the substituted $LaNi_{5-x}M_x$ (M = Co, Mn, Al, Fe, Cu, Sn) or overstochiometric $LaNi_{5+x}$ (x = 0–0.5) compounds leads to a reduction of the strain parameters. Thus, it is natural to propose a similar explanation for the $CeNi_5 \rightarrow CeNi_5D_{6.3}$ transformation; here larger, as compared to the $LaNi_5D_{6.5}$ [9], values of the microstrain parameters developed during the deuteration of the Ce-based intermetallic are caused by significantly larger volume expansion during the deuterium absorption in $CeNi_5$ (30% for $CeNi_5$ vs. 24% for the $LaNi_5$).

3.2. $ZrFe_{2-x}Al_x$–D_2 system

$ZrFe_2$ intermetallic compound crystallizes with C15 ($MgCu_2$) Laves-type structure. For three $ZrFe_{2-x}Al_x$ alloys with x = 0.02; 0.04 and 0.20 synthesized by arc melting, SR XRD studies showed that Fe substitution by Al increases the unit cell parameters while remaining as a FCC crystal structure, from a = 7.072 Å for $ZrFe_2$ [4] to a = 7.08492(8) Å for $ZrFe_{1.98}Al_{0.02}$, a = 7.08658(7) Å for $ZrFe_{1.96}Al_{0.04}$ and a = 7.0978(1) Å for $ZrFe_{1.80}Al_{0.20}$.

The hydrogenation/deuteration properties were studied at deuterium pressures reaching 1600 bar in a Sieverts type volumetric setup in the laboratory and at D_2 pressures up to 1000 bar in the high pressure sample cell for the NPD studies of the deuterides by *in situ* neutron powder diffraction. *In situ* studies demonstrated a very fast kinetics of H/D exchange in the $ZrFe_{2-x}Al_x$ hydrides. The deuterium uptake for $ZrFe_{1.98}Al_{0.02}$ after activation by several hydrogen absorption–desorption cycles, was measured in the laboratory using conventional PCT measurements. The maximum value reached was 3.4 at.D/f.u. (at 1600 bar). This value is very close to the experimentally observed maximum hydrogen absorption capacity of the $ZrFe_2$ intermetallic alloy of 3.5 at.H/f.u. at 1800 bar and room temperature [16]. For the NPD studies, the absorption was performed at room temperature without preliminary activation of the as-cast samples (0.5–1 mm). Because of absence of activation and cycling, and as a result of lower synthesis pressure applied, maximum reached D storage capacity was slightly lower than in the Sieverts 1600 bar D_2 experiment, reaching 3.0 at.D/f.u. for $ZrFe_{1.98}Al_{0.02}$ and 2.9 at.D/f.u. for $ZrFe_{1.96}Al_{0.04}$.

The measurements of the PCT isotherms showed:

(a) A significant effect of aluminium, even at its low content, on the thermodynamics of the hydrogenation/deuteration process of $ZrFe_{2-x}Al_x$. Indeed, as can be seen from Fig. 4b, the midpoint of the plateau for the $\alpha \rightarrow \beta$ transformation during the first deuteration is observed at ~560 bar D_2 for $ZrFe_{1.98}Al_{0.02}$, and at ~410 bar for $ZrFe_{1.96}Al_{0.04}$. These pressures are significantly reduced as compared to the $ZrFe_2$–H_2 system, where the first H absorption plateau at room temperature is above 1 kbar, at 1120 bar [16].

(b) On the second and further absorption cycles, the equilibrium pressure of hydrogen absorption is significantly reduced, to 690 bar for $ZrFe_2$–H_2 [16] and to 430 bar for the $ZrFe_{1.98}Al_{0.02}$–D_2 systems.

(c) A pronounced hysteresis between the D_2 pressures of desorption and absorption during the first charge–discharge cycle. The hysteresis is, however, significantly reduced during the absorption–desorption cycling (see Fig. 4a).

Similar variations in plateau pressures and hysteresis between the first absorption–desorption cycle and further cycles are typical for a number of intermetallic hydrides and were earlier observed for the $LaNi_5$–H_2 [17] and $CeNi_5$–H_2 [8] systems. Such hysteresis was attributed to the extra energy required for the formation of imperfect microstructure via generation of the lattice defects during the first cycle of hydrogen absorption–desorption [8,18]. When a certain level of the defects is reached, the activated microstructure is established, and the PCT isotherms become fully reproducible during the following hydrogenation–dehydrogenation cycles.

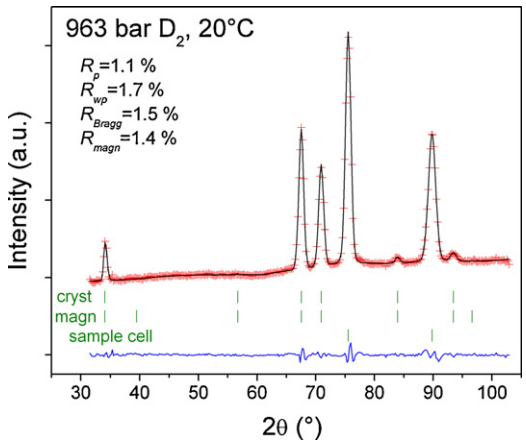

Fig. 5. Neutron powder diffraction pattern for the $ZrFe_{1.98}Al_{0.02}D_3$ deuteride showing observed (+), calculated (—) and difference (bottom line) profiles.

Deuteration resulted in expansion of the unit cells reaching $\Delta V/V = 23.5\%$ ($a = 7.6003(5)$ Å) for $ZrFe_{1.98}Al_{0.02}D_{2.9(1)}$; 23.2% ($a = 7.5966(5)$ Å) for $ZrFe_{1.96}Al_{0.04}D_{2.9(2)}$ and 18.6% for $ZrFe_{1.8}Al_{0.2}D_{2.7(2)}$ ($a = 7.5141(5)$ Å). Deuterium content in the deuterides yielded from Rietveld refinements of the samples studied by *in situ* PND, agrees with the data of the volumetric measurements (Fig. 4b). Detailed data on the studied crystal structures of the $ZrFe_{2-x}Al_x$-based deuterides is given in Table 2. Deuteration proceeds via a formation of a two-phase region α + β, instead of a formation of a continuous solid solution of deuterium in the metal matrix; saturation of the sample with deuterium is reached around 1000 bar D_2 (Fig. 4b).

The refinements of the NPD data (Fig. 5) showed that D atoms occupy the $Zr_2(Fe,Al)_2$ tetrahedra 96 g ($x = 0.32$; $y = x$; $z = 0.13$; occupancy ~24%). Interatomic distances Me–D within the tetrahedra are: $d_{Zr-D} = 2.01–2.08$; $d_{(Fe,Al)-D} = 1.75$ Å. The latter distances do not exclude a possibility of the occupancy of the Al-substituted sites by H/D, as such a distance is in a typical range for the Al–H bonding in the crystal structures of the polymorphs of aluminium hydride, 1.66–1.79 Å [19] (Fig. 6).

From NPD data it was found that initial intermetallic alloys and their corresponding deuterides are ferromagnetic. Magnetic moments of Fe at room temperature for $ZrFe_{1.98}Al_{0.02}$ and $ZrFe_{1.96}Al_{0.04}$ slightly increase from the alloy/D solid solution to the corresponding deuteride, similar to the $ZrFe_2$ based deuteride [4]. Fe replacement by Al slightly decreases the saturation magnetization, which is not significantly temperature-dependent between the temperatures 4.1–320 K (in the field of 100 Oe). Magnetization studies of the initial $ZrFe_{1.98}Al_{0.02}$ alloy showed that its saturation

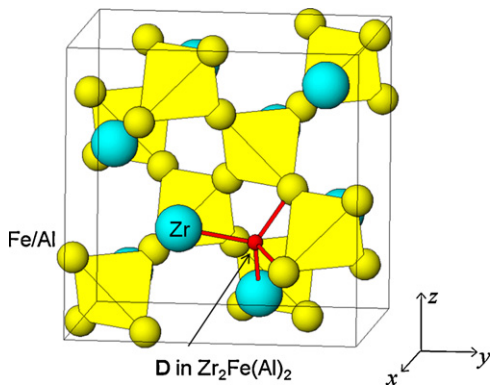

Fig. 6. The crystal structure of the $ZrFe_{2-x}Al_xD_y$ deuteride.

Table 2
Crystallographic data for the $ZrFe_{2-x}Al_x$ ($x = 0.02$; 0.04; 0.20) compounds and their corresponding deuterides at 20 °C. Sp.gr. $Fd\bar{3}m$: Zr in 8a (1/8, 1/8, 1/8); Fe(Al) in 16d (1/2, 1/2, 1/2).

Compositions of the samples and D_2 pressures	a, Å	$\Delta a/a$, %	$\Delta V/V$, %	ΔV/at.D, Å^3	Positional parameters for the D atoms (96g; x, x, z)			M(Fe), μ_B	Interatomic Me–D distances, Å
$ZrFe_{1.98}Al_{0.02}$ [a]	7.08492(8)							1.9(1)	
$ZrFe_{1.98}Al_{0.02}D_{2.9(1)}$ 963 bar	7.6003(4)	7.3	23.5	3.59	$x = 0.319(1)$	$z = 0.126(1)$	occup. 24(1)%	2.2(1)	Zr–D 2.08 Zr–D 2.01 Fe(Al)–D 1.75
$ZrFe_{1.96}Al_{0.04}$ [a]	7.08658(7)							1.89(8)	
$ZrFe_{1.96}Al_{0.04}D_{2.9(2)}$ 989 bar	7.5966(5)	7.2	23.2	3.56	$x = 0.319(1)$	$z = 0.126(1)$	occup. 24(1)%	2.18(6)	Zr–D 2.09 Zr–D 2.00 Fe(Al)–D 1.75
$ZrFe_{1.8}Al_{0.2}$ [a]	7.0978(1)							1.9(1)	
$ZrFe_{1.8}Al_{0.2}D_{2.7(2)}$ 953 bar	7.5141(5)	5.9	18.6	3.09	$x = 0.324(7)$	$z = 0.129(4)$	occup. 23(2)%	1.2(2)	Zr–D 2.11 Zr–D 1.98 Fe(Al)–D 1.70

[a] Lattice parameter for initial alloys obtained from Rietveld refinements of SR XRD data.

magnetization is reached in the applied field of 4 kOe and is equal to 2.55 μ_B/f.u. at room temperature and 3.29 μ_B/f.u. at 4.1 K. However, NPD studies of the $ZrFe_{1.98}Al_{0.02}$ yielded a higher refined value of the magnetic moment on Fe atoms, 3.8(2) μ_B/f.u. The agreement between the magnetization data and the NPD was reached by assuming a ferromagnetic structure with an induced moment of 1.2(2) μ_B on the Zr site and antiparallel alignment of the magnetic moment on Fe and on Zr. On deuteration, the magnetic moment on Fe increases from 1.9 μ_B for $ZrFe_{1.98}Al_{0.02}$ and $ZrFe_{1.96}Al_{0.04}$ to 2.2 μ_B for both $ZrFe_{1.98}Al_{0.02}D_{2.9}$ and $ZrFe_{1.96}Al_{0.04}D_{2.9}$. However, for the alloy with the highest Al content, $ZrFe_{1.8}Al_{0.2}$, the trend is reversed. The magnetic moment on Fe, 1.9 μ_B, decreases to 1.2 μ_B on deuteration.

Similar magnetic structures as observed for $ZrFe_{1.98}Al_{0.02}$ and $ZrFe_{1.98}Al_{0.02}D_{2.9}$ were earlier reported for $ZrFe_2$ [20] and $ZrFe_2D_{2.7}$ [4].

4. Summary and conclusions

This work presents the data of the neutron powder diffraction, pressure–composition–temperature and magnetization measurements studies of two most commonly used groups of the hydrogen storage intermetallics, belonging to Haucke and Laves type compounds, and studied at high hydrogen/deuterium pressures up to 1600 bar. Phase-structural transformations in two studied systems, including $CeNi_5$–D_2 and $ZrFe_{2-x}Al_x$ (x = 0.02; 0.04; 0.20)–D_2, were investigated by *in situ* NPD at pressures up to 1000 bar.

Formation of the saturated $CeNi_5D_{6.3}$ deuteride results in filling of three types of interstices, Ce_2Ni_2, Ni_4, and Ce_2Ni_3 and is accompanied by a very significant volume expansion (30.1%) and a change of Ce valence to Ce^{3+}.

Al substitution for Fe in $ZrFe_2$ to form $ZrFe_{2-x}Al_x$ (x = 0.02; 0.04; 0.20) significantly decreases deuterium absorption pressures and results in a very fast kinetics of H/D exchange in the formed hydrides. Deuterium absorption capacity, hysteresis of H/D absorption and desorption, the unit cell expansion and stability of the hydrides systematically change with Al content. In the $ZrFe_{2-x}Al_x$-based deuterides D atoms exclusively occupy the $Zr_2(Fe,Al)_2$ tetrahedra. Observed interatomic distances are Zr–D = 1.98–2.11; (Fe, Al)–D = 1.70–1.75 Å.

In the $ZrFe_{2-x}Al_x$-based hydrides (x = 0.02; 0.04), hydrogen absorption was found to slightly increase the magnetic moments on the Fe atoms, from 1.9 μ_B at RT for the alloy to 2.2 μ_B at RT for its deuteride.

In conclusion, this work clearly demonstrates a great potential of the *in situ* neutron powder diffraction in probing the mechanism of the hydrogenation to form solid hydrogen storage materials. Neutron scattering at high pressures not only provides an insight into the metal–hydrogen bonding by establishing hydrogen neighborhood and relative population of different sites, but also shows a thermodynamic difference between the hydrogenation and hydrogen desorption processes and changes in the behaviors of cycling of hydrogen uptake and release. Further development of *in situ* NPD studies, particularly in combination with SR XRD of the metal–hydrogen systems, should be considered as a very relevant and important task in discovery and optimization of the novel and advanced hydrogen storage materials.

Acknowledgements

This work has received a support from the Norwegian Research Council.

The authors are grateful for the staff of the Swiss Norwegian Beam Line, ESRF, Grenoble, France for a skillful assistance during the synchrotron XRD experiments.

A possibility to collect neutron powder diffraction data at Institut Laue-Langevin, Grenoble, France (instrument D1B) is gratefully acknowledged.

References

[1] N. Takeichi, H. Senoh, T. Yokota, H. Tsuruta, K. Hamada, H.T. Takeshita, H. Tanaka, T. Kiyobayashi, T. Takano, N. Kuriyama, Int. J. Hydrogen Energy 28 (2003) 1121–1129.
[2] E.H. Kisi, E.MacA. Gray, S.J. Kennedy, J. Alloys Compd. 216 (1994) 123–129.
[3] M.P. Pitt, E.MacA. Gray, Europhys. Lett. 64 (2003) 344–350.
[4] V. Paul-Boncour, F. Bourée-Vigneron, S.M. Filipek, I. Marchuk, I. Jacob, A. Percheron-Guégan, J. Alloys Compd. 356–357 (356) (2003) 69–72.
[5] M. Bereznitsky, I. Jacob, J. Bloch, M.H. Mintz, J. Alloys Compd. 351 (2003) 180–183.
[6] J. Rodriguez-Carvajal, Physica B 192 (1993) 55–69.
[7] V.A. Yartys, R.V. Denys, J.P. Maehlen, C.J. Webb, E.MacA. Gray, T. Blach, A.A. Poletaev, J.K. Solberg, O. Isnard, in: C.M. Wang, N. de Jonge, R.E. Dunin-Borkowski, A. Braun, J.-H. Guo, H. Schober, R.E. Winans (Eds.), Proceedings of the 2010 MRS Spring Meeting/Mater. Res. Soc. Symp. Proc. Volume 1262, San Francisco, USA/Warrendale, PA, April 5–9, 2010 (Paper #: 1262-W04-01, doi:10.1557/PROC-1262-W04-01. ISBN:978-1-60511-239-8).
[8] S.N. Klyamkin, N.S. Zakharkina, J. Alloys Compd. 361 (2003) 200–205.
[9] M. Latroche, J.-M. Joubert, A. Percheron-Guégan, F. Bouree-Vigneron, J. Solid State Chem. 177 (2004) 1219–1229.
[10] P. Fischer, A. Furrer, G. Busch, L. Schlapbach, Helv. Phys. Acta 50 (1977) 421–430.
[11] C. Lartigue, A. Percheron-Guégan, J.C. Achard, J.L. Soubeyroux, J. Less-Common Met. 113 (1985) 127–148.
[12] M.P. Pitt, E.MacA. Gray, E.H. Kisi, B.A. Hunter, J. Alloys Compd. 293–295 (1999) 118–123.
[13] E. Wu, E.H. Kisi, E.MacA. Gray, J. Appl. Crystallogr. 31 (1998) 363–368.
[14] R. Černý, J.-M. Joubert, M. Latroche, A. Percheron-Guégan, K. Yvon, J. Appl. Crystallogr. 33 (2000) 997–1005.
[15] M. Latroche, J. Rodriguez-Carvajal, A. Percheron-Guégan, F. Bourée-Vigneron, J. Alloys Compd. 218 (1995) 64–72.
[16] T. Zotov, E. Movlaev, S. Mitrokhin, V. Verbetsky, J. Alloys Compd. 459 (2008) 220–224.
[17] C.E. Buckley, E.MacA. Gray, E.H. Kisi, J. Alloys Compd. 215 (1994) 195.
[18] K. Nomura, H. Uruno, S. Ono, S. Suda, J. Less-Common Met. 107 (1985) 221–230.
[19] J. Graetz, J.J. Reilly, V.A. Yartys, J.P. Maehlen, B.M. Bulychev, V.E. Antonov, B.P. Tarasov, I.E. Gabis, J. Alloys Compd. 509 (2011) S517–S528.
[20] P. Warren, J.B. Forsyth, G.B. McIntyre, N. Bernhoeft, J. Phys.: Condens. Matter 4 (1992) 5795–5800.